




# TgIF2K-B Is an eIF2 $\alpha$ Kinase in *Toxoplasma gondii* That Responds to Oxidative Stress and Optimizes Pathogenicity

Leonardo Augusto,<sup>a,b\*</sup> Jennifer Martynowicz,<sup>c</sup> Parth H. Amin,<sup>a</sup> Kenneth R. Carlson,<sup>a</sup> Ronald C. Wek,<sup>a</sup>  William J. Sullivan, Jr.<sup>b,c</sup>

<sup>a</sup>Department of Biochemistry & Molecular Biology, Indiana University School of Medicine, Indianapolis, Indiana, USA

<sup>b</sup>Department of Pharmacology & Toxicology, Indiana University School of Medicine, Indianapolis, Indiana, USA

<sup>c</sup>Department of Microbiology & Immunology, Indiana University School of Medicine, Indianapolis, Indiana, USA

**ABSTRACT** *Toxoplasma gondii* is an obligate intracellular parasite that persists in its vertebrate hosts in the form of dormant tissue cysts, which facilitate transmission through predation. The parasite must strike a balance that allows it to disseminate throughout its host without killing it, which requires the ability to properly counter host cell defenses. For example, oxidative stress encountered by *Toxoplasma* is suggested to impair parasite replication and dissemination. However, the strategies by which *Toxoplasma* mitigates oxidative stress are not yet clear. Among eukaryotes, environmental stresses induce the integrated stress response via phosphorylation of a translation initiation factor, eukaryotic initiation factor 2 (eIF2). Here, we show that the *Toxoplasma* eIF2 kinase TgIF2K-B is activated in response to oxidative stress and affords protection. Knockout of the TgIF2K-B gene,  $\Delta$ *tgif2k-b*, disrupted parasite responses to oxidative stresses and enhanced replication, diminishing the ability of the parasite to differentiate into tissue cysts. In addition, parasites lacking TgIF2K-B exhibited resistance to activated macrophages and showed greater virulence in an *in vivo* model of infection. Our results establish that TgIF2K-B is essential for *Toxoplasma* responses to oxidative stress, which are important for the parasite's ability to establish persistent infection in its host.

**IMPORTANCE** *Toxoplasma gondii* is a single-celled parasite that infects nucleated cells of warm-blooded vertebrates, including one-third of the human population. The parasites are not cleared by the immune response and persist in the host by converting into a latent tissue cyst form. Development of tissue cysts can be triggered by cellular stresses, which activate a family of TgIF2 kinases to phosphorylate the eukaryotic translation initiation factor TgIF2 $\alpha$ . Here, we establish that the TgIF2 kinase TgIF2K-B is activated by oxidative stress and is critical for maintaining oxidative balance in the parasite. Depletion of TgIF2K-B alters gene expression, leading to accelerated growth and a diminished ability to convert into tissue cysts. This study establishes that TgIF2K-B is essential for the parasite's oxidative stress response and its ability to persist in the host as a latent infection.

**KEYWORDS** Apicomplexa, *Toxoplasma*, differentiation, oxidative stress, parasites, stress response, translation, translational control

*Toxoplasma gondii* is a protozoan parasite that infects nucleated cells of warm-blooded vertebrates, including up to one-third of the human population (1). *Toxoplasma* is an obligate intracellular pathogen that replicates inside a parasitophorous vacuole (tachyzoites) that forms an interface between the parasites and their host cell (2). One of the features that facilitated *Toxoplasma's* omnipresence in the animal kingdom is the ability to persist in its host as latent tissue cysts (bradyzoites) that serve to disseminate the parasite to new hosts via predation (3). *Toxoplasma* has thus evolved mechanisms to balance parasite metabolism, replication, and cyst formation

**Citation** Augusto L, Martynowicz J, Amin PH, Carlson KR, Wek RC, Sullivan WJ, Jr. 2021. TgIF2K-B is an eIF2 $\alpha$  kinase in *Toxoplasma gondii* that responds to oxidative stress and optimizes pathogenicity. *mBio* 12:e03160-20. <https://doi.org/10.1128/mBio.03160-20>.

**Editor** Louis M. Weiss, Albert Einstein College of Medicine

**Copyright** © 2021 Augusto et al. This is an open-access article distributed under the terms of the [Creative Commons Attribution 4.0 International license](https://creativecommons.org/licenses/by/4.0/).

Address correspondence to Ronald C. Wek, [rwek@iu.edu](mailto:rwek@iu.edu), or William J. Sullivan, [wjsullivan@iu.edu](mailto:wjsullivan@iu.edu).

\* Present address: Leonardo Augusto, Department of Pathology & Microbiology, University of Nebraska Medical Center, Omaha, Nebraska, USA.

**Received** 5 November 2020

**Accepted** 1 December 2020

**Published** 26 January 2021

to allow rapid dissemination and encystment throughout host tissues without killing the host (4).

In addition to facilitating transmission, tissue cysts afford *Toxoplasma* protection from immune defenses, thus preventing the parasite from being eliminated from the host. However, a consequence of *Toxoplasma* persistence as a cyst is diminished parasite replication. Rapidly proliferating tachyzoites respond to environmental stresses by slowing parasite growth and by triggering differentiation into bradyzoites (3). A critical inverse relationship between the rate of cell proliferation and resistance to environmental stresses has been noted among other unicellular eukaryotes (5). This balance provides *Toxoplasma* with resistance to physiological and environmental stresses and ensures optimal infection and transmission into new hosts.

An important mechanism for mitigating stress damage in eukaryotes is the integrated stress response (ISR). The ISR features a family of related protein kinases that phosphorylate the  $\alpha$  subunit of eukaryotic initiation factor 2 (eIF2 $\alpha$ ) in response to a variety of stresses. Phosphorylation of eIF2 $\alpha$  damps global translation, which conserves nutrients and energy while promoting preferential expression of genes involved in stress remediation (6). Phosphorylation of *Toxoplasma* eIF2 $\alpha$  (TgIF2 $\alpha$ -P) occurs in response to environmental stresses and is a contributing factor in the formation of tissue cysts (7, 8). Four TgIF2 $\alpha$  kinases have been identified in the parasite, designated A through D (9). TgIF2K-A is localized to the parasite endoplasmic reticulum (ER) and responds to perturbations in this organelle, processes analogous to those of the eIF2 $\alpha$  kinase PERK (EIFAK3/PEK) (10). TgIF2K-C and -D are related the eIF2 $\alpha$  kinase GCN2 (EIFAK4) and respond to amino acid starvation and stresses of the extracellular environment, respectively (11–13). The function of TgIF2K-B remains unknown.

In this study, we addressed the functions of TgIF2K-B in *Toxoplasma* replication, stress responses, and pathogenesis. As *Toxoplasma* is an aerobic parasite that needs to limit molecular damage caused by generation of excessive reactive oxygen species (14), including those generated by host defense mechanisms (15), we hypothesized that TgIF2K-B functions in antioxidation responses. We generated a genetic knockout for use in *in vitro* and *in vivo* host model systems to show that TgIF2K-B is essential for the activation of catalase antioxidative responses, which affects tachyzoite replication and bradyzoite conversion. Our results suggest that control of antioxidant responses is central to the parasite's growth rate, which is a critical determinant in the ability of the parasite to persist in its host in a latent form. We conclude that TgIF2K-B is a novel sensor protein governing the rate of *Toxoplasma* replication and cyst formation through translational control mechanisms involving TgIF2 $\alpha$  phosphorylation.

## RESULTS

**Knockout of TgIF2K-B accelerates *Toxoplasma* replication.** We showed previously that TgIF2K-B is localized to the parasite cytosol and can phosphorylate TgIF2 $\alpha$  *in vitro* (8). To address stress activation of TgIF2K-B and the role of this eIF2 $\alpha$  kinase in parasite physiology and differentiation, we generated knockout clones in the type II ME49 strain using CRISPR (clustered regularly interspaced short palindromic repeats)/Cas9 methods (16). The knockout strategy involved genetic insertion of a modified allele of the gene encoding dihydrofolate reductase (DHFR), which confers resistance to pyrimethamine, into the first exon of the *TgIF2K-B* locus (17) (Fig. 1A). PCR primers upstream of the insertion cassette (P1) were used to amplify the genomic sequences and primers inside the DHFR gene and in the *TgIF2K-B* gene were used to amplify across the DHFR insertion (P2). The PCR products indicated the anticipated DHFR insertion, generating ME49  $\Delta$ *tgif2k-b* parasites (Fig. 1B). In addition, we confirmed the loss of *TgIF2K-B* mRNA and protein in the  $\Delta$ *tgif2k-b* parasites by RT-qPCR (Fig. 1C) and by immunoblotting using a specific antibody (8) (Fig. 1D).

It was noted that parasite clones lacking TgIF2K-B appeared to grow faster than the wild type (WT), which was confirmed by counting the number of parasites per vacuole in infected human foreskin fibroblasts (HFFs). We counted parasites at 24 and 36 h

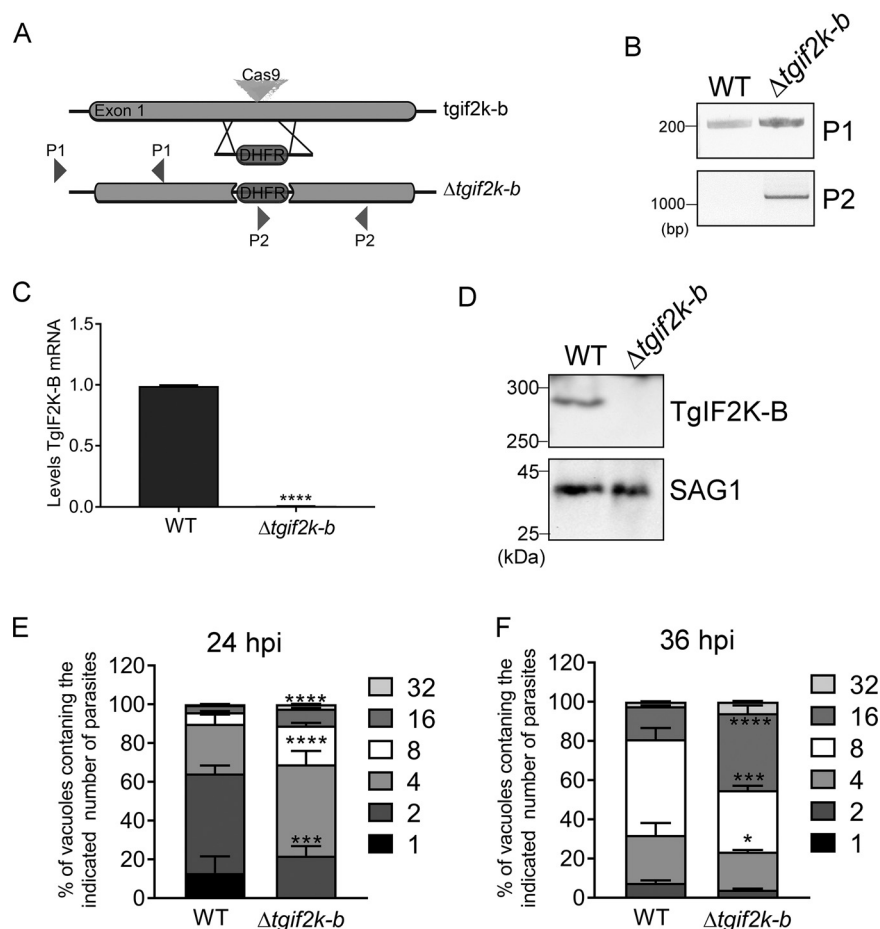


**FIG 1** Disruption of *TgIF2K-B* in ME49 strain accelerates replication. (A) Strategy used to the disrupt the *TgIF2K-B* gene involved using CRISPR/Cas9 to insert a modified *DHFR* allele that encodes pyrimethamine resistance into exon 1. The indicated primers pairs, P1 and P2, were used to confirm the disrupted locus in drug-resistant clones. (B) Genomic DNA isolated from WT and  $\Delta$ *tgif2k-b* parasites was used to assess structure of *TgIF2K-B* locus by PCR with primer pairs P1 and P2. PCR products were separated by agarose gel electrophoresis, and the sizes of bands are given in base pairs. (C) Levels of *TgIF2K-B* mRNA were measured by RT-qPCR for WT and  $\Delta$ *tgif2k-b* parasites (values are means and SD;  $n=3$ ). (D) Immunoblot of WT and  $\Delta$ *tgif2k-b* lysates for TgIF2K-B protein. SAG1 protein was probed as a loading control. Molecular weights are given in kilodaltons. At 24 (E) and 36 h (F) postinfection, the number of parasites in 250 random vacuoles was counted, and values are percentages of the total number of vacuoles examined (with SD;  $n=3$ ). \*,  $P < 0.05$ ; \*\*\*,  $P < 0.005$ ; \*\*\*\*,  $P < 0.0001$ .

postinfection, finding that  $\Delta$ *tgif2k-b* parasites outpaced WT at each time point (Fig. 1E and F). These results suggest that the TgIF2K-B pathway plays a role in the regulation of parasite replication. Attempts to complement  $\Delta$ *tgif2k-b* parasites were problematic due to the length of the *TgIF2K-B* gene (8.4 kb); however, a second independent *TgIF2K-B* gene knockout clone phenocopied the original, supporting the idea that the reported effects are due to the disruption of the *TgIF2K-B* locus (data not shown).

**TgIF2K-B participates in the oxidative stress response.** To address the function of TgIF2K-B during infection and assess which stress condition(s) activates TgIF2K-B, we treated WT and  $\Delta$ *tgif2k-b* parasites with the following stress agents: thapsigargin (TG), an ER stress inducer that leads to activation of TgIF2K-A (10), halofuginone (HF), which inhibits the aminoacylation of tRNA<sup>Pro</sup> and is also a potent inducer of the eIF2 $\alpha$  kinase GCN2, and sodium arsenite (Ars), which triggers general oxidative stress. Extracellular parasites were used to ensure that the observed effects were due to direct consequences of the stress on the parasites and not indirect effects through the host cell. We detected increased levels of TgIF2 $\alpha$ -P in WT parasites exposed to each of the

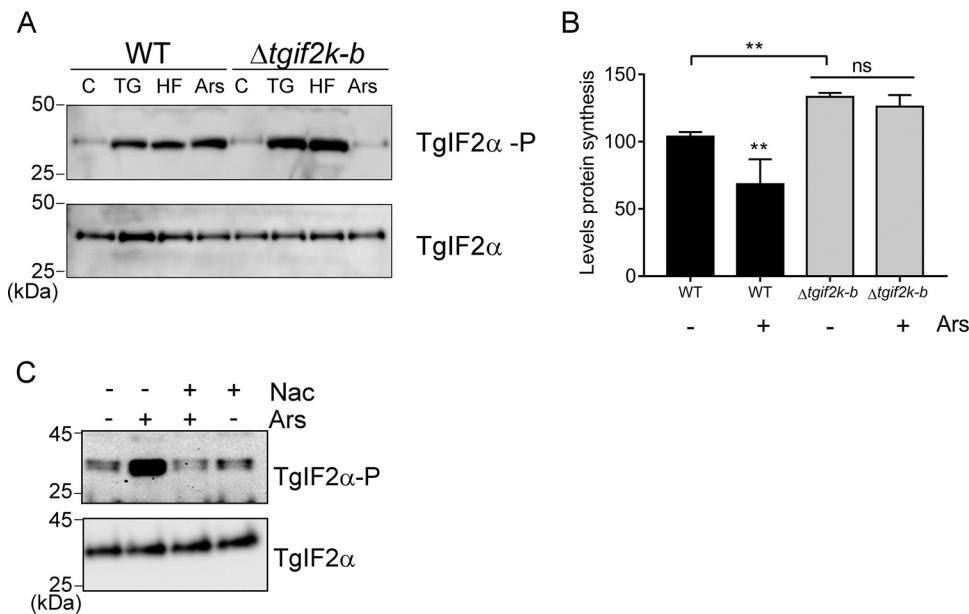


**FIG 2** TgIF2K-B responds to oxidative stress. (A) Extracellular WT and  $\Delta$ tgif2k-b tachyzoites were treated with 1  $\mu$ M thapsigargin (TG), 50 nM halofuginone (HF), or 5  $\mu$ M sodium arsenite (Ars) for 2 h at 37°C. Parasites were harvested, and the levels of phosphorylated TgIF2 $\alpha$  (TgIF2 $\alpha$ -P) and total TgIF2 $\alpha$  were measured by immunoblotting. (B) WT and  $\Delta$ tgif2k-b tachyzoites were exposed to 5  $\mu$ M Arsenite or vehicle for 2 h and then treated with puromycin for 15 min. Lysates were then analyzed by immunoblotting with puromycin-specific antibody. Levels of translation were quantified using densitometry and normalized to total TgIF2 $\alpha$  for each respective lane. Levels of translation are presented in a bar graph (means and SD;  $n=3$ ). \*\*,  $P < 0.01$ ; ns = not significant. (C) WT parasites were treated with 5  $\mu$ M Arsenite for 2 h in the presence or absence of 20  $\mu$ M N-acetylcysteine (Nac); TgIF2 $\alpha$ -P and total TgIF2 $\alpha$  were then assessed by immunoblotting.

three different stress conditions (Fig. 2A). In contrast,  $\Delta$ tgif2k-b parasites displayed minimal levels of TgIF2 $\alpha$ -P upon treatment with arsenite (Ars), whereas the other stress conditions showed robust TgIF2 $\alpha$ -P (Fig. 2A). As expected after phosphorylation of TgIF2 $\alpha$ , global protein synthesis was lowered by arsenite stress in WT parasites; however, it remained unaffected in  $\Delta$ tgif2k-b parasites exposed to arsenite (Fig. 2B; also, see Fig. S1 in the supplemental material). Also of note is the higher level of basal protein synthesis in  $\Delta$ tgif2k-b parasites compared to WT, consistent with the demands of faster replication (Fig. 2B). In support of the idea that oxidative stress induced by arsenite is critical for induction of TgIF2 $\alpha$ -P, cotreatment of the parasites with arsenite and the antioxidant N-acetylcysteine (NAC) led to a sharp decrease in TgIF2 $\alpha$ -P levels in the WT parasites (Fig. 2C). We conclude that TgIF2K-B is an eIF2 $\alpha$  kinase activated by oxidative stress in *Toxoplasma*.

To address the transcriptome changes resulting from TgIF2K-B deletion, we performed transcriptome sequencing (RNA-seq) analyses of WT and  $\Delta$ tgif2k-b parasites. Differentially expressed genes in  $\Delta$ tgif2k-b parasites were selected using  $\log_2$  fold change of  $\leq \pm 1$  or  $\geq \pm 1$  and  $P$  values of  $\leq 0.05$  as detailed in Materials and Methods. Loss of TgIF2K-B resulted in induction of 1,162 genes and lowered expression of 1,686 genes relative to WT parasites (Fig. 3A and B, Table S2). The RNA-seq analyses showed that loss of TgIF2K-B led to enhanced levels of *Toxoplasma* superoxide dismutase-1 (*TgSOD1*) mRNA and downregulation of genes related to antioxidation, including PRX2 and thioredoxin (Fig. 3A). These results suggest that TgIF2K-B directs expression of genes involved in mitigating oxidative damage.

It is noteworthy that loss of TgIF2K-B resulted in upregulation of 311 genes involved in protein synthesis, including 117 ribosome-related genes, whereas 6 ribosome-related genes were downregulated (Fig. 3B). These results further support the idea that there are higher levels of protein synthesis in  $\Delta$ tgif2k-b parasites that would contribute to increased replication (Fig. 1E and F and 2B). Furthermore, the absence of TgIF2K-B

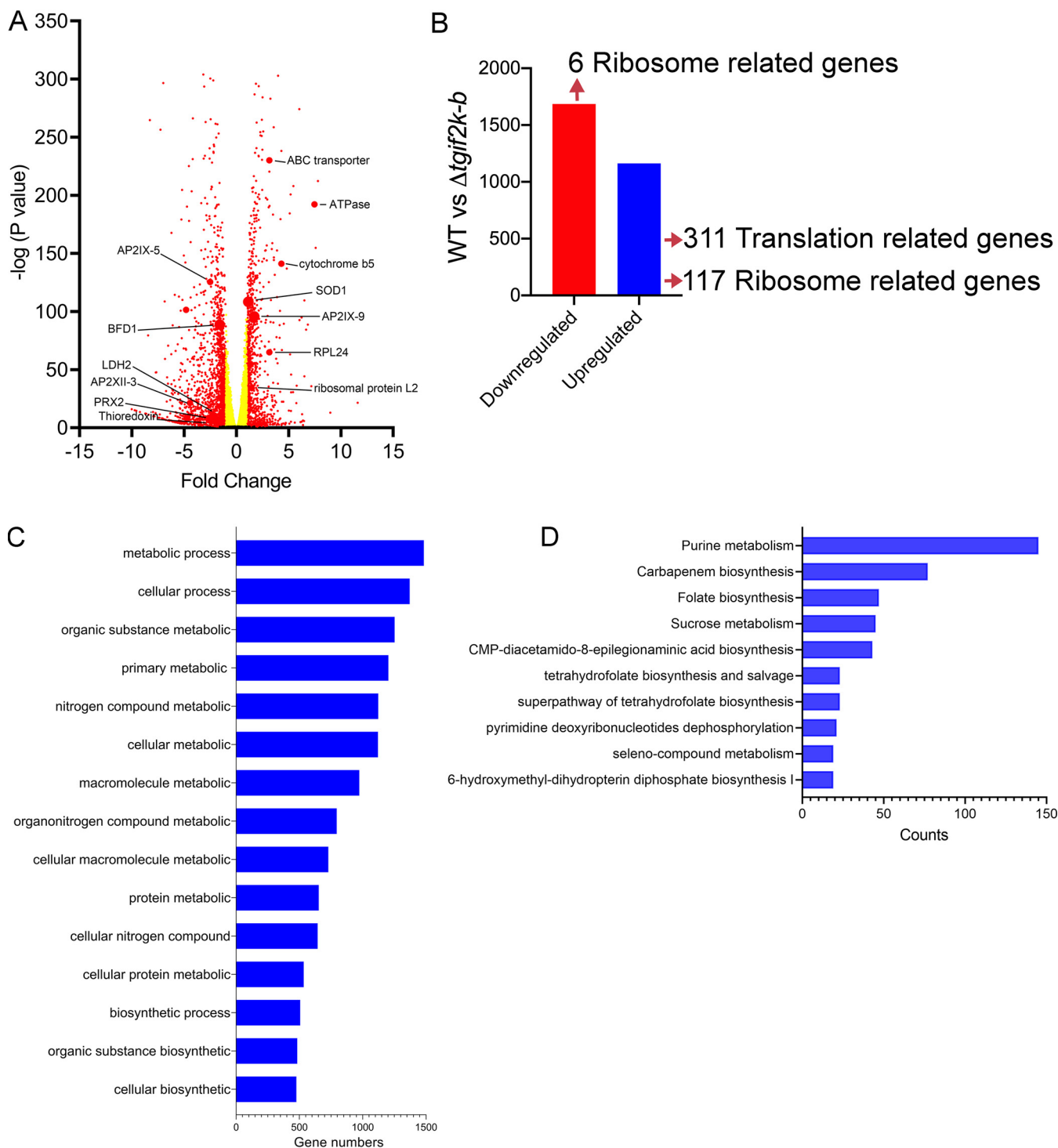


**FIG 3** RNA-seq analysis of WT and  $\Delta tgif2k-b$  parasites. RNA-seq and differential expression of genes in  $\Delta tgif2k-b$  parasites compared to WT parasites. (A) Volcano plots showing transcription profile of  $\Delta tgif2k-b$  parasites compared to WT parasites. (B) Number of up- and downregulated genes in WT versus  $\Delta tgif2k-b$  parasites; 1,162 genes were identified as significantly upregulated (blue) and 1,686 genes as significantly downregulated (red) in  $\Delta tgif2k-b$  parasites. The analyses were based on biological replicates using fold change of 1.0 and a  $P$  value of  $\leq 0.05$ . (C) Gene ontology enrichment analysis for biological processes (using ToxoDB) of upregulated genes in  $\Delta tgif2k-b$  compared to WT parasites. (D) Gene ontology enrichment analysis for metabolic pathways (using ToxoDB) of upregulated genes in  $\Delta tgif2k-b$  parasites. In panels C and D, the lengths of the bars indicate the numbers of genes identified for the indicated processes and pathways.

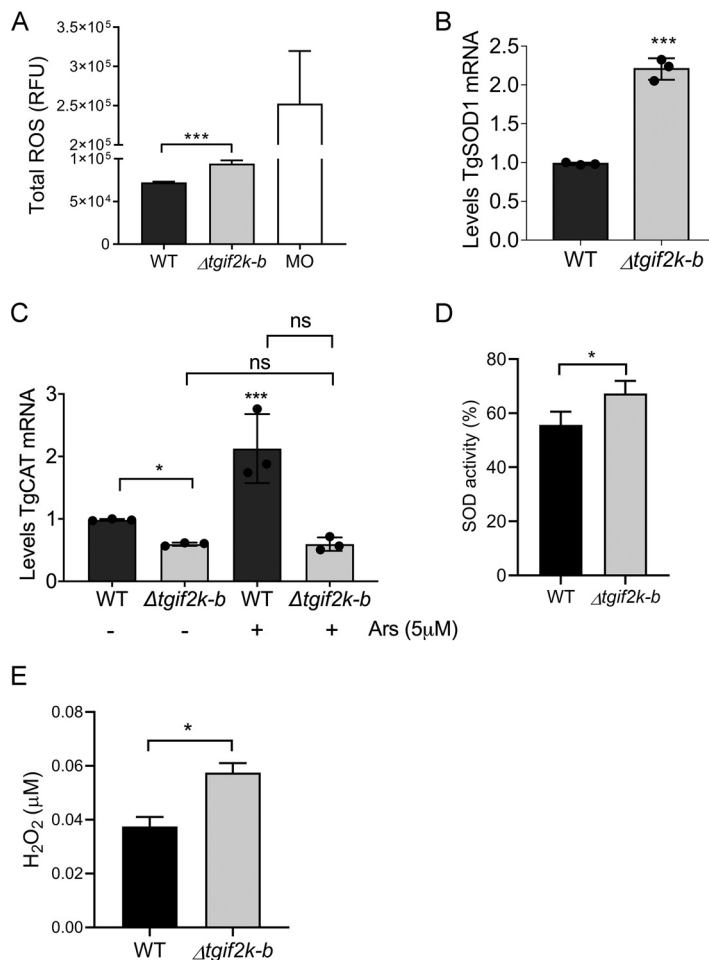


**FIG 4** Loss of TgIF2K-B disrupts the antioxidant response. (A) Reactive species (14) were measured in WT and  $\Delta$ tgif2k-b parasites using OxiSelect ROS/RNS; values were normalized to total protein (given as means and SD;  $n=3$ ). WT parasites were treated with monensin (MO; 1 ng/ml) for 30 min as a positive control. (B) *TgSOD1* mRNA levels were measured by RT-qPCR in WT and  $\Delta$ tgif2k-b parasites (given as means and SD;  $n=3$ ). (C) *TgCAT* mRNA levels were measured by RT-qPCR in WT and  $\Delta$ tgif2k-b parasites subjected to 5  $\mu$ M Ars or vehicle for 2 h at 37°C (values are means and SD;  $n=3$ ). (D) Superoxide dismutase activity in WT and  $\Delta$ tgif2k-b parasites (means and SD;  $n=3$ ). (E) Hydrogen peroxide concentration in WT and  $\Delta$ tgif2k-b parasites (means and SD;  $n=3$ ). \*,  $P < 0.05$ ; \*\*\*,  $P < 0.005$ ; ns, not significant.

resulted in enhanced expression of more than 1,000 genes involved in metabolic processes, including those involved in purine and carbohydrate metabolism and folate biosynthesis (Fig. 3C and D; Fig. S2 and S3).

To more fully address the redox functions of TgIF2K-B, we measured reactive oxygen species (ROS) levels in WT and knockout parasites, using monensin as a positive control. Results indicate that deletion of TgIF2K-B leads to significantly higher levels of ROS than in WT parasites (Fig. 4A). It has been suggested that ROS act as second messengers regulating the balance between cell proliferation and cell cycle (18, 19). An early step in antioxidation responses involves SOD, which generates H<sub>2</sub>O<sub>2</sub> that will subsequently be decomposed by catalase into oxygen and water. We first measured *TgSOD1* mRNA levels by reverse transcriptase quantitative PCR (RT-qPCR), confirming that they are enhanced in  $\Delta$ tgif2k-b parasites, as detected in the RNA-seq (Fig. 3A and 4B). We next measured expression of catalase (*TgCAT*) mRNA in WT and  $\Delta$ tgif2k-b parasites after treatment with sodium arsenite for 2 h. While WT parasites exhibit increased *TgCAT* mRNA levels upon arsenite treatment,  $\Delta$ tgif2k-b parasites fail to do so (Fig. 4C). Consistent with the changes in mRNA expression, we found that the activity of SOD is



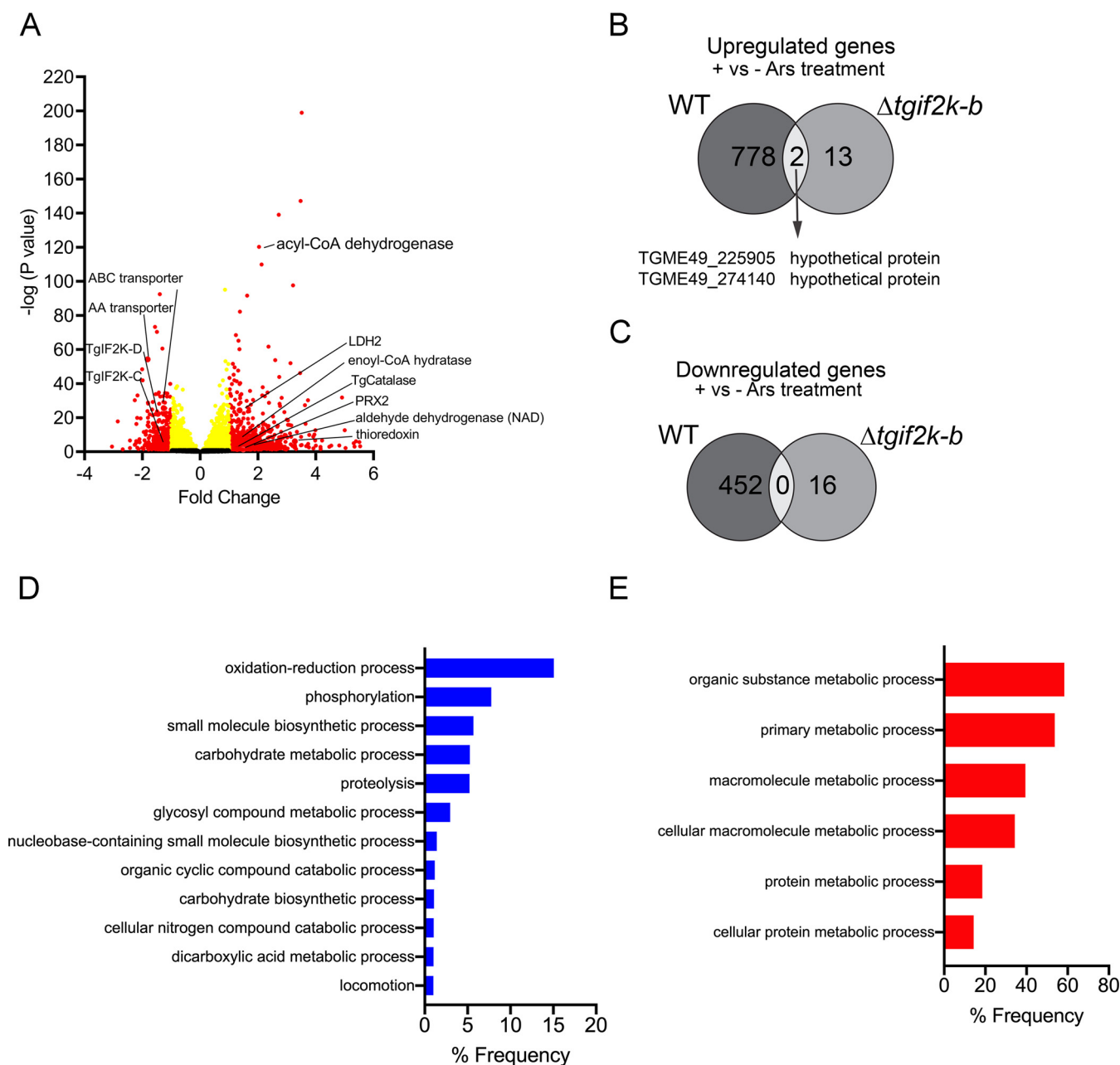


**FIG 5** RNA-seq analysis of WT and  $\Delta tgif2k-b$  parasites treated with sodium arsenite. (A) Volcano plots showing transcription profile of WT parasites treated with Ars for 2 h compared to WT parasites untreated. (B and C) WT and  $\Delta tgif2k-b$  parasites were treated with arsenite or vehicle for 2 h and processed for RNA-seq. Numbers of differentially expressed genes were compared between WT and  $\Delta tgif2k-b$  parasites with and without arsenite. Gene Ontology enrichment analysis was used to identify cellular processes that were upregulated (D) or downregulated (E) in WT parasites with and without arsenite.

higher in  $\Delta tgif2k-b$  parasites than WT parasites (Fig. 4D). Furthermore, we detected an increased concentration of  $H_2O_2$  in parasites lacking TgIF2K-B (Fig. 4E). Together, these results support the idea that TgIF2K-B activation and phosphorylation of TgIF2 $\alpha$  alter expression of antioxidant genes.

To address the transcriptome changes upon arsenite treatment and determine the contributions of TgIF2K-B to this gene expression network, we treated extracellular WT and  $\Delta tgif2k-b$  tachyzoites for 2 h with 5  $\mu M$  arsenite and then performed RNA-seq analyses. The analyses indicated that the expression of 780 genes was enhanced in WT parasites in response to arsenite treatment and 452 genes were downregulated (Fig. 5A to C, Table S3). A major cell process enhanced in WT parasites in response to arsenite involves oxidation-reduction (Fig. 5D, Table S5), including induction of catalase, as

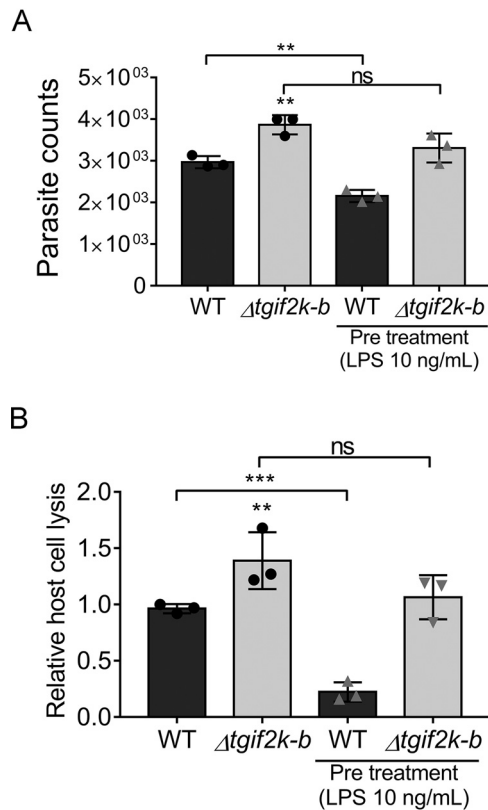


**FIG 6** TgIF2K-B governs parasite replication in macrophages. (A) Tachyzoites were allowed to infect J774.1 macrophages that were activated by LPS for 24 h. Four days postinfection, parasite replication was measured using the PCR-based B1 assay (values are means and SD;  $n=3$ ). (B) Tachyzoites were cycled through activated macrophages for 2 days before being harvested by syringe lysis to then inoculate HFF monolayers. After 6 days, the degree of HFF host cell lysis was quantified (values are means and SD;  $n=3$ ). \*\*,  $P < 0.01$ , \*\*\*,  $P < 0.001$ ; ns, not significant.

noted above (Fig. 4C). In contrast, a majority of genes downregulated by arsenite treatment in WT parasites are involved in metabolism, including genes related to acetyl coenzyme A (acetyl-CoA) carboxylase, glycosyl transferase, beta-ketoacyl-acyl carrier protein synthase, beta-ketoacyl-acyl carrier protein synthase, and amino acid transporters (Fig. 5E and Table S4). We also compared the RNA-seq analyses between WT and  $\Delta$ tgif2k-b parasites in response to arsenite treatment. In sharp contrast to the hundreds of genes altered in the WT response,  $\Delta$ tgif2k-b parasites upregulated only 15 genes and downregulated 16 genes (Fig. 5B and C). WT and  $\Delta$ tgif2k-b parasites shared only 2 genes that were upregulated in response to arsenite (Fig. 5B). The results emphasize that the loss of TgIF2K-B greatly dysregulates the parasite's response to oxidative stress.

**Loss of TgIF2K-B leads to parasite resistance during macrophage infection.** We next investigated how the compromised ability to respond to oxidative stress might affect parasites in macrophages, which produce ROS as a defense mechanism against *Toxoplasma* (20, 21). We addressed this by analyzing replication of WT and  $\Delta$ tgif2k-b parasites in activated macrophages. Prior to infection, we stimulated J774.1 macrophages with lipopolysaccharide (LPS) for 24 h; we then quantified the number of intracellular parasites 4 days postinfection. Unlike HFFs, parasites inside macrophages are difficult to count, so they were quantified using the PCR-based B1 assay (22). While the number of WT parasites was significantly decreased in activated macrophages, replication of  $\Delta$ tgif2k-b parasites was unimpeded (Fig. 6A). We also found that  $\Delta$ tgif2k-b parasites showed diminished TgIF2 $\alpha$  phosphorylation compared to WT parasites following infection of activated macrophages (Fig. S4). These results suggest that TgIF2K-B is



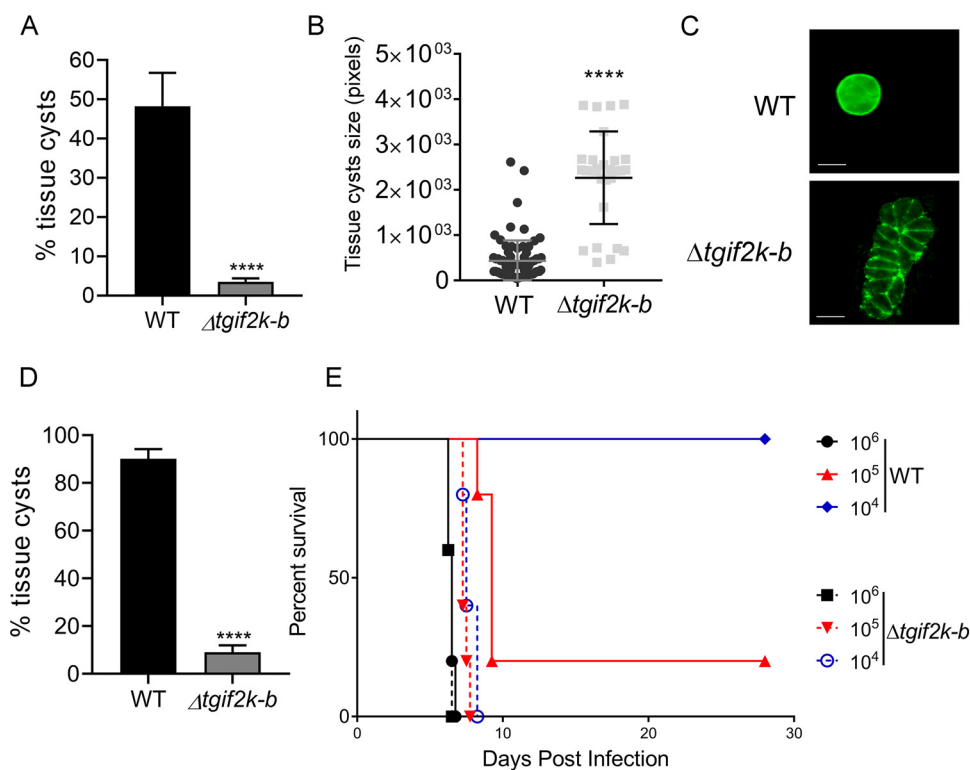


**FIG 7** Effects of TgIF2K-B on tissue cyst formation. (A) WT or  $\Delta tgif2k-b$  parasites were prompted to spontaneously differentiate in HFF cells. After 5 days, rhodamine-conjugated *Dolichos biflorus* agglutinin (DBA) lectin was used to visualize and count tissue cysts (values are means and SD;  $n=3$ ). (B) The area of 100 tissue cysts (in pixels) was measured using ImageJ software (values are means and SD;  $n=3$ ). (C) Tissue cysts formed by WT or  $\Delta tgif2k-b$  parasites after 5 days of alkaline stress were visualized by immunofluorescence assay (IFA) with DBA lectin (green). Bar = 10  $\mu$ m. (D) WT or  $\Delta tgif2k-b$  parasites were prompted to differentiate in HFF cells using conventional alkaline stress for 4 days and quantified as described for panel A (values are means and SD;  $n=3$ ). (E) Female BALB/c mice (5 per group) were infected by intraperitoneal injection with  $10^4$ ,  $10^5$ , and  $10^6$  of WT or  $\Delta tgif2k-b$  tachyzoites as indicated. Infected mice were monitored at least 3 times per day, and percent survival was recorded. \*\*\*,  $P < 0.005$ ; \*\*\*\*,  $P < 0.001$ .

important for sensing oxidative stress generated by host immune cells, and the inability to do so allows tachyzoite replication to proceed unfettered.

In addition, we measured parasite viability following infection of macrophages that had been activated and those that had not. Mock- or LPS-stimulated J774.1 macrophages were infected with WT or  $\Delta tgif2k-b$  parasites for 2 days, at which point parasites were harvested and used to infect an HFF cell monolayer (Fig. 6B). After 6 days, the area of parasite plaques in the HFF monolayer was measured for each condition. Results show that cycling through macrophages significantly reduced HFF infectivity of WT tachyzoites, but the  $\Delta tgif2k-b$  parasites displayed resistance to this insult (Fig. 6B). The effect was more pronounced when the parasites were cycled through activated macrophages. These findings further support the idea that TgIF2K-B senses oxidative stresses and triggers a response that slows parasite growth to manage the stress.

**TgIF2K-B is a sensor protein governing replication rate and cyst formation.** As phosphorylation of TgIF2 $\alpha$  accompanies bradyzoite differentiation and tissue cyst formation (8), we hypothesized that parasites lacking TgIF2K-B may show deficits in tissue cyst formation. WT and  $\Delta tgif2k-b$  parasites were allowed to spontaneously differentiate in HFF cells. After 5 days,  $\Delta tgif2k-b$  cultures contained <5% tissue cysts whereas WT cultures contained ~50% (Fig. 7A). Vacuoles containing  $\Delta tgif2k-b$  parasites were twice the size of those produced by WT parasites; moreover, clear *Dolichos biflorus* lectin staining indicative of a cyst wall was rarely evident (Fig. 7B and C). We also performed an analysis of tissue cyst formation following alkaline stress, which is a potent trigger

of bradyzoite differentiation *in vitro*. WT parasites formed robust tissue cysts at a frequency of ~90%, whereas only ~10% of  $\Delta$ *tgif2k-b* parasites showed evidence of cyst wall formation (Fig. 7D). These results suggest that TgIF2K-B is a critical sensor that balances developmental transitions between replication and latency.

To address the importance of TgIF2K-B *in vivo*, we infected BALB/c mice with increasing doses of WT or  $\Delta$ *tgif2k-b* tachyzoites. The lack of TgIF2K-B had a profound effect on pathogenesis in the mouse model: BALB/c mice tolerate a dose of  $10^4$  WT parasites, but none of the mice were able to survive the equivalent dose of  $\Delta$ *tgif2k-b* tachyzoites (Fig. 7E). These results mirror the augmented replication rate of  $\Delta$ *tgif2k-b* tachyzoites seen *in vitro* and further underscore the relevance of TgIF2K-B as a sensor of *in vivo* signals that trigger conversion to latent forms.

## DISCUSSION

The ability of *Toxoplasma* to persist in its host as latent tissue cysts is a key feature that has greatly enhanced the transmission of the parasite. Tissue cysts remain infectious and allow the parasite to infect new hosts via predation. Conversion of tachyzoites to bradyzoites can occur spontaneously in certain cell backgrounds (23) or following exposure to a wide variety of cellular stresses (3). We previously linked the phosphorylation of parasite eIF2 $\alpha$  with stress-induced bradyzoite development and latency stages in *Toxoplasma* and its fellow apicomplexan parasite *Plasmodium* (9). Four eIF2 $\alpha$  kinases have been identified in *Toxoplasma* that respond to ER and nutrient stresses, but the function of TgIF2K-B, which has no clear counterpart in other eukaryotes, had yet to be resolved. Here, we report the discovery that TgIF2K-B contributes to the management of the parasite's response to oxidative stress.

ROS are a natural consequence of cellular metabolism and have been reported to regulate cellular growth rate. Cells must have systems in place to sense ROS and adapt accordingly. As arsenicals induce ROS that generate oxidative stress, we examined the response of *Toxoplasma* to sodium arsenite. Exposure of the parasites to arsenite induced translational control, as evidenced by TgIF2 $\alpha$  phosphorylation and diminished protein synthesis (Fig. 2). Using a CRISPR/Cas9 approach, we successfully generated a genetic knockout of TgIF2K-B, which failed to phosphorylate TgIF2 $\alpha$  in response to oxidative stress. The ability to initiate translational control in response to ER and nutritive stresses remained unaffected in  $\Delta$ *tgif2k-b* parasites.

$\Delta$ *tgif2k-b* parasites exhibited a higher replication rate than WT parasites. We performed an RNA-seq analysis under normal culture conditions and found abnormal transcriptome changes in  $\Delta$ *tgif2k-b* parasites that featured gene networks involved in protein synthesis and cellular metabolism, consistent with the enhanced parasite replication that was also observed (Fig. 1E and 3). We postulated that the accelerated growth may stem from increased levels of ROS, which have been reported to serve as secondary messengers that influence replication rate in other species (18). Notably,  $\Delta$ *tgif2k-b* parasites showed significant increases in ROS in the absence of added stress (Fig. 4A). The precise association between ROS levels and proliferation rate is an unresolved question for future investigation.

Abnormal alterations in gene expression occurred between WT and  $\Delta$ *tgif2k-b* parasites in response to arsenite treatment as well. RNA-seq analysis revealed that loss of TgIF2K-B resulted in dysregulation of oxidation-reduction processes upon arsenite exposure (Fig. 5). The data suggest that without TgIF2K-B, parasites fail to sense oxidative stress and consequently do not slow growth to adapt to this response. Such a phenotype would not be expected to be viable over time; indeed,  $\Delta$ *tgif2k-b* parasites have been observed to revert to normal growth rates after prolonged culture through an unresolved mechanism (data not shown). Together, these results indicate that TgIF2K-B is central for the management of oxidative stress in *Toxoplasma*, a process that is linked to parasite replication.

It is curious that with loss of translational control and sharply altered mRNA expression,  $\Delta$ *tgif2k-b* parasites showed increased replication in infected HFF (Fig. 1E and F)

and in activated macrophages (Fig. 6). There was also enhanced morbidity in mice infected with  $\Delta$ *tgif2k-b* parasites compared with those infected with WT parasites, consistent with the faster replication of the former (Fig. 7E). Our RNA-seq analysis provides mechanistic insights into why tachyzoite replication is enhanced and cyst formation diminished in  $\Delta$ *tgif2k-b* parasites. For example, *AP2IX-9* is a transcriptional repressor that restricts development of the tissue cyst; its increased expression in  $\Delta$ *tgif2k-b* parasites would inhibit the expression of bradyzoite mRNAs. Similarly, *TgBFD1* is a master regulator that drives bradyzoite differentiation (24); its decreased expression in  $\Delta$ *tgif2k-b* parasites would be expected to impair tissue cyst formation. Bradyzoite-specific genes like that for LDH2 were also decreased in  $\Delta$ *tgif2k-b* parasites relative to WT parasites. Consistent with these observations, the loss of TgIF2K-B significantly lowered the frequency of tissue cyst conversion *in vitro*; moreover, the few cyst-like structures that did form were larger and contained more parasites (Fig. 7). In combination with the observed higher replication rates of  $\Delta$ *tgif2k-b* parasites, these results suggest that loss of TgIF2K-B dysregulates the transcriptional program essential for triggering parasite differentiation.

These results indicate that TgIF2K-B contributes to growth plasticity that enables *Toxoplasma* to appropriately lower the replication rate in response to oxidative stress. To achieve stress adaptation, there is an inverse correlation in unicellular eukaryotes between growth rate and stress survival (5). Diminished growth rates during stress are critical for appropriate modulation of gene expression and redistribution of resources to best mediate stress tolerance. In the case of *Toxoplasma*, a critical mode of stress adaptation involves differentiation into bradyzoite cysts, a clinically relevant process that is compromised in  $\Delta$ *tgif2k-b* parasites.

The phenotypes associated with loss of TgIF2K-B are representative of antagonistic pleiotropy (25), where the gene regulates multiple traits. Enhanced replication is a beneficial trait associated with  $\Delta$ *tgif2k-b* parasites, but it comes at the expense of the parasite being able to modulate proliferation when faced with signals to transition into latent stages. Therefore, TgIF2K-B functions as a critical sensor to balance parasite replication and latency; parasites lacking TgIF2K-B would likely have reduced transmission through the predation route due to their compromised ability to form infectious tissue cysts.

## MATERIALS AND METHODS

**Parasite culture.** ME49 tachyzoites were cultivated in human foreskin fibroblast (HFF; ATCC) monolayers in Dulbecco modified Eagle medium (DMEM) supplemented with 5% heat-inactivated fetal bovine serum (FBS) (Gibco/Invitrogen), 100 U/ml penicillin, and 100  $\mu$ g/ml streptomycin. HFFs were cultivated in DMEM supplemented with 10% FBS. The cultures were maintained in a humidified incubator at 37°C with 5% CO<sub>2</sub>.

**Disruption of *TgIF2K-B* genomic locus.** The  $\Delta$ *tgif2k-b* parasites were generated by disrupting the genomic locus using CRISPR/Cas9 and an associated guide targeting the sequence ACCTCTCGCTCT GCCTTCCT to allow integration of a minigene encoding a modified dihydrofolate reductase (DHFR) that confers pyrimethamine resistance (16, 17). The pSAG1:U6-Cas9:sgRNA-TgIF2K-B vector was generated using Q5 site-directed mutagenesis (New England Biolabs) (26) and the listed forward and reverse primers (Table S1). After transfection, the parasites were selected using 1  $\mu$ M pyrimethamine for three passages before cloning by limited dilution in 96-well plates. Independent clones were selected and assayed by PCR using primer pairs indicated in Fig. 1A.

**Immunoblotting for TgIF2K-B.** Parasites were purified from HFFs using a 3- $\mu$ m filter, and lysates were made by suspension of the parasite pellets in a phosphate-buffered saline (PBS) solution supplemented with 0.01% Triton X-100. Proteins in parasite lysates were resolved with NuPAGE using 4 to 12% gradient bis-Tris polyacrylamide gels (Thermo Fisher Scientific). Separated proteins were then transferred from the gels to a nitrocellulose membrane. Immunoblotting was performed using antibody specific to TgIF2K-B (8) diluted 1:10 in blocking solution (Tris-buffered saline [TBS], pH 7.4, with Tween 20 and 2.5% bovine serum albumin [BSA]). The secondary antibody, goat anti-rabbit IgG (heavy plus light chain [H+L]) conjugated to horseradish peroxidase (HRP), was used at a dilution of 1:1,000. After washing, the membrane was incubated with Pierce enhanced chemiluminescence (ECL) immunoblot substrate to visualize the proteins levels using the FluorChem E system (Protein Simple).

**Measurements of mRNA levels.** RNA was isolated from parasites using TRIzol LS (Invitrogen), and cDNA was generated using Omniscript (Qiagen). RT-qPCR was carried out using specific primers (Table S1) with SYBR green real-time PCR master mixes (Invitrogen) and the StepOnePlus Real system (Applied Biosystems). Relative levels of transcripts were calculated with the  $\Delta\Delta$ C<sub>t</sub> method using the GAPDH gene as an internal control. Each experiment was performed three times, each with three technical replicates.

**Measurements of TgIF2 $\alpha$  phosphorylation.** Tachyzoites were purified from infected HFFs by syringe passage and filtration as described in reference 27 and then incubated in DMEM supplemented

with 5% FBS in the presence of a stress agent or vehicle: 1  $\mu$ M thapsigargin (TG; Sigma-Aldrich), 50 nM halofuginone (HF; Sigma-Aldrich), or 5  $\mu$ M sodium arsenite (Ars; Sigma-Aldrich), for 2 h at 37°C. For some reactions, 20  $\mu$ M *N*-acetylcysteine (NAC; Sigma-Aldrich) was added. Parasites were lysed in PBS containing 0.01% Triton X-100, supplemented with the protease inhibitor cocktail cComplete and an EDTA-free protease inhibitor cocktail (Roche). Total protein levels were quantified using a Pierce bicinchoninic acid (BCA) protein assay kit (Thermo-Fisher). Proteins were separated by NuPAGE on 4 to 12% bis-Tris gels (Thermo Fisher Scientific) and transferred to a nitrocellulose membrane for immunoblot analyses using antibodies recognizing total TgIF2 $\alpha$  or phosphorylated TgIF2 $\alpha$  (1:1,000) (27). The secondary antibodies, goat anti-rabbit IgG (H+L) conjugated to HRP, were used at a 1:5,000 dilution. After washing, the membranes were incubated with Pierce ECL substrate to visualize the proteins.

**Parasite replication assays.** Tachyzoites were allowed to invade HFF monolayers for 2 h. Infected cultures were then washed and incubated with fresh culture medium. At 24 and 36 h postinfection, infected HFF monolayers were fixed with 2.5% paraformaldehyde for 20 min and then blocked with PBS supplemented with 2% BSA. Cells were incubated with anti-SAG1 (Invitrogen) in blocking buffer containing 0.2% Triton X-100 for 1 h. Next, goat anti-mouse Alexa-Fluor 488 (Invitrogen) was applied for 1 h, followed by ProLong Gold antifade mountant with 4',6-diamidino-2-phenylindole (DAPI) to visualize parasites. The number of parasites in 250 randomly selected vacuoles was counted for each sample. All samples were anonymized prior to parasite counting.

J774.1 macrophages (ATCC) were incubated with 10 ng/ml of LPS for 24 h before being infected with tachyzoites for 2 h at an MOI of 3 (28). Following 4 days of infection, cells were harvested and the numbers of parasites were quantified using the PCR-based B1 assay (22). To test parasite fitness in HFFs after cycling through macrophages, infected macrophages were harvested by scraping and syringe lysis at 2 days postinfection. The same volume of medium containing tachyzoites was then used to infect an HFF monolayer for 2 h, which was then washed with DMEM twice. Six days postinfection, the degree of host cell lysis was determined by crystal violet staining as described previously (29).

**Puromycin incorporation.** To determine the levels of protein synthesis in WT and  $\Delta$ *tgif2k-b* parasites, extracellular tachyzoites were exposed to 5  $\mu$ M arsenite for 2 h. Parasites were then incubated with 10  $\mu$ g/ml puromycin (Sigma) for 15 min, and parasites were lysed in PBS containing 0.01% Triton X-100. Total protein synthesis was measured by immunoblotting using the antipuromycin antibody at 1:500 (EMD Millipore). Protein synthesis was quantified by densitometry using ImageJ on each lane and normalized by immunoblot using antibody specific to steady-state levels of TgIF2 $\alpha$  protein (13).

**RNA preparation and sequencing.** Tachyzoites were allowed to invade HFF monolayers for 2 h; then, infected monolayers were washed, and the medium was replaced with fresh medium. At 36 h postinfection, intracellular tachyzoites were harvested from HFFs by syringe passage and filtering. Parasites were then washed in DMEM and centrifuged at 300  $\times$  *g* for 15 min. Purified extracellular WT and  $\Delta$ *tgif2k-b* tachyzoites were treated with vehicle or 5  $\mu$ M sodium arsenite for 2 h at 37°C, and total RNA was extracted using RNeasy (Qiagen). The RNA concentration for each sample was measured using Nanodrop One (Thermo Scientific). Library preparation and sequencing was performed by GENEWIZ (South Plainfield, NJ) using an Illumina HiSeq instrument with 150-bp paired-end reads. Three biological replicates were included in each of the untreated test groups, and four biological replicates were included in each treated test group. The quality of the raw sequencing reads obtained from GENEWIZ was checked using FastQC (30), and the low-quality reads were trimmed using TrimGalore (31). Trimmed reads were aligned to the reference *T. gondii* ME49 genome (<https://toxodb.org/toxo/app>) using hierarchical indexing for spliced alignment of transcripts (HISAT2) with default parameters (32). We obtained 335,646,715 read pairs in total, of which 269,152,478 mapped uniquely to the *Toxoplasma* genome (80.2%). Trimming, quality filtering, and alignment were all performed using the high-throughput computing cluster Karst and the Data Capacitor II high-performance file system, both of which are available to all Indiana University researchers. The numbers of reads aligning to the exons of different genes were counted using featureCounts (33). Last, differential expression analysis was carried out using DESeq2 with default parameters except that genes with total counts less than 10 across all samples were discarded (34). Volcano plots were created using R (35), and genes with a log<sub>2</sub> fold change of  $\geq \pm 1$  and *P* value of  $\leq 0.05$  were considered significant for further network analyses. Gene Ontology enrichment analyses were performed using the collated genes that were significantly upregulated or downregulated, with a focus on molecular and biological cellular processes.

**Reactive oxygen species.** ROS were measured using the OxiSelect *in vitro* ROS/RNS assay kit (Cell Biolabs, Inc.) per the manufacturer's instructions. Briefly, lysates from 10<sup>7</sup> parasites were added to a 96-well plate, followed by 50  $\mu$ l of the catalyst reagent in the kit. Reaction mixtures were incubated for 5 min at room temperature before the addition of 2',7'-dichlorofluorescein (DCFH) solution into each well for 1 h incubation. Fluorescence was measured at 480 nm/530 nm (excitation/emission wavelengths) in a Synergy H1 microplate reader (BioTek). All samples were assayed in triplicate. Parasites were treated with monensin (MO; 1 ng/ml) for 30 min as a positive control.

**Superoxide dismutase activity and H<sub>2</sub>O<sub>2</sub> measurement.** ME49 WT and  $\Delta$ *tgif2k-b* tachyzoites were purified from infected HFFs by syringe passage and filtration. Parasites were then lysed in ice cold Tris-HCl, pH 7.4, containing 0.02% Triton X-100 and supplemented with cComplete protease inhibitor cocktail (Roche), and the lysate was clarified by centrifugation at 14,000  $\times$  *g* for 5 min at 4°C. The supernatant was then used to measure superoxide dismutase (SOD) activity using a superoxide dismutase activity assay kit (Colorimetric) following the manufacturer's instructions (Abcam). The activity of SOD was measured using this colorimetric method as the optical density at 450 (OD<sub>450</sub>) and compared to a standard curve.

To measure H<sub>2</sub>O<sub>2</sub> levels, purified parasites were resuspended in buffer (150 mM NaCl, 50 mM Tris-Cl, pH 7.4) supplemented with cComplete protease inhibitor cocktail (Roche) and sonicated. For

deproteinization, 4 M perchloric acid (PCA) was added to a final concentration of 1 M in the homogenate solution, followed by protein precipitation and centrifugation. The supernatant was then used in a hydrogen peroxide assay kit as per the manufacturer's instructions (Abcam). The reaction mixture was incubated at room temperature for 10 min; then each well was measured at excitation/emission wavelengths of 535/587 nm. The values of each well were compared to a standard curve to determine H<sub>2</sub>O<sub>2</sub> concentration.

**Bradyzoite differentiation assays.** ME49 tachyzoites were allowed to infect HFF monolayers for 2 h. After washing and replacing the medium with DMEM–5% FBS, infected cells were cultured at 37°C or subjected to the bradyzoite induction triggers alkaline stress and CO<sub>2</sub> deprivation. To visualize tissue cyst walls, infected cells were fixed with 2.5% paraformaldehyde and stained with rhodamine-conjugated *Dolichos biflorus* agglutinin (Vector Laboratories). Tissue cysts were counted in 250 randomly chosen infected cells and considered positive if there was a clear indication of *D. biflorus* agglutinin staining at the former PVM (parasitophorous vacuole membrane), indicating cyst wall formation. Tissue cyst area was measured using ImageJ by drawing a region of interest (ROI). All samples were anonymized prior to counting.

**Analysis of infection in mice.** Five- to six-week-old female BALB/c mice were purchased from The Jackson Laboratory (Bar Harbor, ME) and allowed to acclimate in our facility for 1 week. Following acclimation, the mice were randomized on the basis of weight into six groups ( $n = 5$ ). WT or  $\Delta$ *tgif2k-b* tachyzoites were prepared in sterile PBS and intraperitoneally injected into the mice, which were then monitored at least 3 times a day. The mice used in this study were housed in American Association for Accreditation of Laboratory Animal Care (AAALAC)-approved facilities at the IUSM Laboratory Animal Research Center (LARC). The Institutional Animal Care and Use Committee (IACUC) at Indiana University School of Medicine approved the use of all animals and procedures (IACUC protocol number 11376).

**Quantification and statistical analysis.** Quantitative data are presented as the means and standard deviations (SD) from biological triplicates. Statistical significance was determined using one-way analysis of variance (ANOVA) with Tukey's *post hoc* test or multiple *t* test two-tailed in Prism (version 7) software (GraphPad Software, Inc., La Jolla, CA). The number of biological replicates ( $n$ ) and *P* values are given in the figure legends. For immunoblot analyses, the reported images are representative of at least three independent experiments.

**Data availability.** RNA-seq data sets from this study are available in the NCBI GEO database (accession number GSE158231).

## SUPPLEMENTAL MATERIAL

Supplemental material is available online only.

**FIG S1**, TIF file, 1.1 MB.

**FIG S2**, TIF file, 0.6 MB.

**FIG S3**, TIF file, 1.3 MB.

**FIG S4**, TIF file, 0.3 MB.

**TABLE S1**, XLSX file, 0.01 MB.

**TABLE S2**, XLSX file, 1.1 MB.

**TABLE S3**, XLSX file, 0.9 MB.

**TABLE S4**, XLSX file, 0.7 MB.

**TABLE S5**, XLSX file, 0.01 MB.

## ACKNOWLEDGMENTS

This research was supported by a research grant from the National Institutes of Health (AI124723 to W.J.S. and R.C.W.). This research was also supported in part by Lilly Endowment, Inc., through its support for the Indiana University Pervasive Technology Institute, and in part by the Indiana METACyt Initiative. The Indiana METACyt Initiative at IU was also supported in part by Lilly Endowment, Inc. This material is based upon work supported by the National Science Foundation under grant no. CNS-0521433.

R.C.W. has received grant support from Eli Lilly and Company and is a scientific advisor to HiberCell. The other authors declare no conflicts of interest.

We thank the Biology of Intracellular Pathogens Group at IUSM and other members of the Wek laboratory for helpful discussions and suggestions.

## REFERENCES

- Halonon SK, Weiss LM. 2013. Toxoplasmosis. *Handb Clin Neurol* 114:125–145. <https://doi.org/10.1016/B978-0-444-53490-3.00008-X>.
- Coppens I, Romano JD. 2018. Hostile intruder: *Toxoplasma* holds host organelles captive. *PLoS Pathog* 14:e1006893. <https://doi.org/10.1371/journal.ppat.1006893>.
- Jeffers V, Tampaki Z, Kim K, Sullivan WJ, Jr. 2018. A latent ability to persist: differentiation in *Toxoplasma gondii*. *Cell Mol Life Sci* 75:2355–2373. <https://doi.org/10.1007/s00018-018-2808-x>.
- White MW, Radke JR, Radke JB. 2014. *Toxoplasma* development—turn the switch on or off? *Cell Microbiol* 16:466–472. <https://doi.org/10.1111/cmi.12267>.
- Zakrzewska A, van Eikenhorst G, Burggraaff JE, Vis DJ, Hoefsloot H,



- Delneri D, Oliver SG, Brul S, Smits GJ. 2011. Genome-wide analysis of yeast stress survival and tolerance acquisition to analyze the central trade-off between growth rate and cellular robustness. *Mol Biol Cell* 22:4435–4446. <https://doi.org/10.1091/mbc.E10-08-0721>.
6. Wek RC. 2018. Role of eIF2 $\alpha$  kinases in translational control and adaptation to cellular stress. *Cold Spring Harb Perspect Biol* 10:a032870. <https://doi.org/10.1101/cshperspect.a032870>.
  7. Zhang M, Joyce BR, Sullivan WJ, Jr, Nussenzweig V. 2013. Translational control in *Plasmodium* and *Toxoplasma* parasites. *Eukaryot Cell* 12:161–167. <https://doi.org/10.1128/EC.00296-12>.
  8. Narasimhan J, Joyce BR, Naguleswaran A, Smith AT, Livingston MR, Dixon SE, Coppens I, Wek RC, Sullivan WJ, Jr. 2008. Translation regulation by eukaryotic initiation factor-2 kinases in the development of latent cysts in *Toxoplasma gondii*. *J Biol Chem* 283:16591–16601. <https://doi.org/10.1074/jbc.M800681200>.
  9. Holmes MJ, Augusto LDS, Zhang M, Wek RC, Sullivan WJ, Jr. 2017. Translational control in the latency of apicomplexan parasites. *Trends Parasitol* 33:947–960. <https://doi.org/10.1016/j.pt.2017.08.006>.
  10. Joyce BR, Tampaki Z, Kim K, Wek RC, Sullivan WJ, Jr. 2013. The unfolded protein response in the protozoan parasite *Toxoplasma gondii* features translational and transcriptional control. *Eukaryot Cell* 12:979–989. <https://doi.org/10.1128/EC.00021-13>.
  11. Wek RC, Jiang HY, Anthony TG. 2006. Coping with stress: eIF2 kinases and translational control. *Biochem Soc Trans* 34:7–11. <https://doi.org/10.1042/BST20060007>.
  12. Konrad C, Wek RC, Sullivan WJ, Jr. 2014. GCN2-like eIF2 $\alpha$  kinase manages the amino acid starvation response in *Toxoplasma gondii*. *Int J Parasitol* 44:139–146. <https://doi.org/10.1016/j.ijpara.2013.08.005>.
  13. Konrad C, Wek RC, Sullivan WJ, Jr. 2011. A GCN2-like eukaryotic initiation factor 2 kinase increases the viability of extracellular *Toxoplasma gondii* parasites. *Eukaryot Cell* 10:1403–1412. <https://doi.org/10.1128/EC.05117-11>.
  14. Roskoski R, Jr. 2016. Classification of small molecule protein kinase inhibitors based upon the structures of their drug-enzyme complexes. *Pharmacol Res* 103:26–48. <https://doi.org/10.1016/j.phrs.2015.10.021>.
  15. Ding M, Kwok LY, Schlüter D, Clayton C, Soldati D. 2004. The antioxidant systems in *Toxoplasma gondii* and the role of cytosolic catalase in defence against oxidative injury. *Mol Microbiol* 51:47–61. <https://doi.org/10.1046/j.1365-2958.2003.03823.x>.
  16. Shen B, Brown K, Long S, Sibley LD. 2017. Development of CRISPR/Cas9 for efficient genome editing in *Toxoplasma gondii*. *Methods Mol Biol* 1498:79–103. [https://doi.org/10.1007/978-1-4939-6472-7\\_6](https://doi.org/10.1007/978-1-4939-6472-7_6).
  17. Donald RG, Roos DS. 1993. Stable molecular transformation of *Toxoplasma gondii*: a selectable dihydrofolate reductase-thymidylate synthase marker based on drug-resistance mutations in malaria. *Proc Natl Acad Sci U S A* 90:11703–11707. <https://doi.org/10.1073/pnas.90.24.11703>.
  18. Sauer H, Wartenberg M, Hescheler J. 2001. Reactive oxygen species as intracellular messengers during cell growth and differentiation. *Cell Physiol Biochem* 11:173–186. <https://doi.org/10.1159/000047804>.
  19. Fehér A, Otvös K, Pasternak TP, Szandtner AP. 2008. The involvement of reactive oxygen species (ROS) in the cell cycle activation (G<sub>0</sub>-to-G<sub>1</sub> transition) of plant cells. *Plant Signal Behav* 3:823–826. <https://doi.org/10.4161/psb.3.10.5908>.
  20. Moreira-Souza ACA, Almeida-da-Silva CLC, Rangel TP, Rocha GDC, Bellio M, Zamboni DS, Vommaro RC, Coutinho-Silva R. 2017. The P2X7 receptor mediates *Toxoplasma gondii* control in macrophages through canonical NLRP3 inflammasome activation and reactive oxygen species production. *Front Immunol* 8:1257. <https://doi.org/10.3389/fimmu.2017.01257>.
  21. Arsenijevic D, Bilbao FD, Giannakopoulos P, Girardier L, Samec S, Richard D. 2001. A role for interferon-gamma in the hypermetabolic response to murine toxoplasmosis. *Eur Cytokine Netw* 12:518–527.
  22. Kompalic-Cristo A, Frotta C, Suarez-Mutis M, Fernandes O, Britto C. 2007. Evaluation of a real-time PCR assay based on the repetitive B1 gene for the detection of *Toxoplasma gondii* in human peripheral blood. *Parasitol Res* 101:619–625. <https://doi.org/10.1007/s00436-007-0524-9>.
  23. Lüder CGK, Rahman T. 2017. Impact of the host on *Toxoplasma* stage differentiation. *Microb Cell* 4:203–211. <https://doi.org/10.15698/mic2017.07.579>.
  24. Waldman BS, Schwarz D, Wadsworth MH, 2nd, Saeji JP, Shalek AK, Lourido S. 2020. Identification of a master regulator of differentiation in *Toxoplasma*. *Cell* 180:359–372.E16. <https://doi.org/10.1016/j.cell.2019.12.013>.
  25. Russell ES, Fondal EL, Coulombre JL. 1948. Preliminary analysis of pleiotropism at the W-locus in the mouse. *Genetics* 33:627.
  26. Behnke MS, Khan A, Sibley LD. 2015. Genetic mapping reveals that sinefungin resistance in *Toxoplasma gondii* is controlled by a putative amino acid transporter locus that can be used as a negative selectable marker. *Eukaryot Cell* 14:140–148. <https://doi.org/10.1128/EC.00229-14>.
  27. Augusto L, Martynowicz J, Staschke KA, Wek RC, Sullivan WJ, Jr. 2018. Effects of PERK eIF2 $\alpha$  kinase inhibitor against *Toxoplasma gondii*. *Antimicrob Agents Chemother* 62:e01442-18. <https://doi.org/10.1128/AAC.01442-18>.
  28. Saito S, Matsuura M, Hirai Y. 2006. Regulation of lipopolysaccharide-induced interleukin-12 production by activation of repressor element GA-12 through hyperactivation of the ERK pathway. *Clin Vaccine Immunol* 13:876–883. <https://doi.org/10.1128/CI.00075-06>.
  29. Roos DS, Donald RG, Morrisette NS, Moulton AL. 1994. Molecular tools for genetic dissection of the protozoan parasite *Toxoplasma gondii*. *Methods Cell Biol* 45:27–63. [https://doi.org/10.1016/s0091-679x\(08\)61845-2](https://doi.org/10.1016/s0091-679x(08)61845-2).
  30. Wingett SW, Andrews S. 2018. FastQ Screen: a tool for multi-genome mapping and quality control. *F1000Res* 7:1338. <https://doi.org/10.12688/f1000research.15931.2>.
  31. Lindgreen S. 2012. AdapterRemoval: easy cleaning of next-generation sequencing reads. *BMC Res Notes* 5:337. <https://doi.org/10.1186/1756-0500-5-337>.
  32. Kim D, Langmead B, Salzberg SL. 2015. HISAT: a fast spliced aligner with low memory requirements. *Nat Methods* 12:357–360. <https://doi.org/10.1038/nmeth.3317>.
  33. Liao Y, Smyth GK, Shi W. 2014. featureCounts: an efficient general purpose program for assigning sequence reads to genomic features. *Bioinformatics* 30:923–930. <https://doi.org/10.1093/bioinformatics/btt656>.
  34. Love MI, Huber W, Anders S. 2014. Moderated estimation of fold change and dispersion for RNA-seq data with DESeq2. *Genome Biol* 15:550. <https://doi.org/10.1186/s13059-014-0550-8>.
  35. R Core Team. 2014. R: a language and environment for statistical computing. <http://www.R-project.org/>.